INTERFACE

rsif.royalsocietypublishing.org

Research

Cite this article: Waldrop LD, Hann M, Henry AK, Kim A, Punjabi A, Koehl MAR. 2015 Ontogenetic changes in the olfactory antennules of the shore crab, *Hemigrapsus oregonensis*, maintain sniffing function during growth. *J. R. Soc. Interface* **12**: 20141077. http://dx.doi.org/10.1098/rsif.2014.1077

Received: 26 September 2014
Accepted: 27 October 2014

Subject Areas:
biomechanics

Keywords:
olfaction, crab, scaling, ontogeny, fluid dynamics, aesthetasc

Author for correspondence:
Lindsay D. Waldrop
e-mail: lwaldrop@email.unc.edu

THE ROYAL SOCIETY PUBLISHING

Ontogenetic changes in the olfactory antennules of the shore crab, *Hemigrapsus oregonensis*, maintain sniffing function during growth

Lindsay D. Waldrop[1,2], Miranda Hann[2], Amy K. Henry[2,3], Agnes Kim[2], Ayesha Punjabi[2] and M. A. R. Koehl[2]

[1]Department of Mathematics, University of North Carolina, CB# 3250, Chapel Hill, NC 27599-3250, USA
[2]Department of Integrative Biology, University of California, Berkeley, CA, USA
[3]Committee on Evolutionary Biology, University of Chicago, Chicago, IL, USA

Malacostracan crustaceans capture odours using arrays of chemosensory hairs (aesthetascs) on antennules. Lobsters and stomatopods have sparse aesthetascs on long antennules that flick with a rapid downstroke when water flows between the aesthetascs and a slow return stroke when water is trapped within the array (sniffing). Changes in velocity only cause big differences in flow through an array in a critical range of hair size, spacing and speed. Crabs have short antennules bearing dense arrays of flexible aesthetascs that splay apart during downstroke and clump together during return. Can crabs sniff, and when during ontogeny are they big enough to sniff? Antennules of *Hemigrapsus oregonensis* representing an ontogenetic series from small juveniles to adults were used to design dynamically scaled physical models. Particle image velocimetry quantified fluid flow through each array and showed that even very small crabs capture a new water sample in their arrays during the downstroke and retain that sample during return stroke. Comparison with isometrically scaled antennules suggests that reduction in aesthetasc flexural stiffness during ontogeny, in addition to increase in aesthetasc number and decrease in relative size, maintain sniffing as crabs grow. Sniffing performance of intermediate-sized juveniles was worse than for smaller and larger crabs.

1. Introduction

Many animals rely on odours (chemical cues carried in the ambient fluid) as a source of information throughout their lives. For example, malacostracan crustaceans use odours to track and locate food, avoid predation, identify conspecifics and mediate reproduction [1–11].

In order to use chemical information in the surrounding water or air, animals must first capture odorant molecules from the ambient fluid [12–14]. During odour capture, many types of animals move fluid currents through specialized olfactory organs such as noses or antennae, or move those organs through the surrounding fluid, thereby transporting odorants close to olfactory receptors. Malacostracans flick through the water the lateral filaments of their olfactory antennules (first antennae; figures 1 and 2), which bear arrays of chemosensory hairs called aesthetascs. It has long been thought that antennule flicking increases the flow of water near the aesthetascs, thereby bringing odour-bearing water closer to the receptor cells in those chemosensory hairs [13,15–17].

Previous research has shown that antennule flicking by lobsters and stomatopods is 'sniffing', i.e. capturing discrete samples of odour-containing fluid [13,17], although the morphologies and kinematics of these animals' antennules differ substantially from those of crabs. A sniff provides a 'snapshot' of an olfactory environment that animals can use to resolve spatial and temporal patterns of chemical signals [18–23].

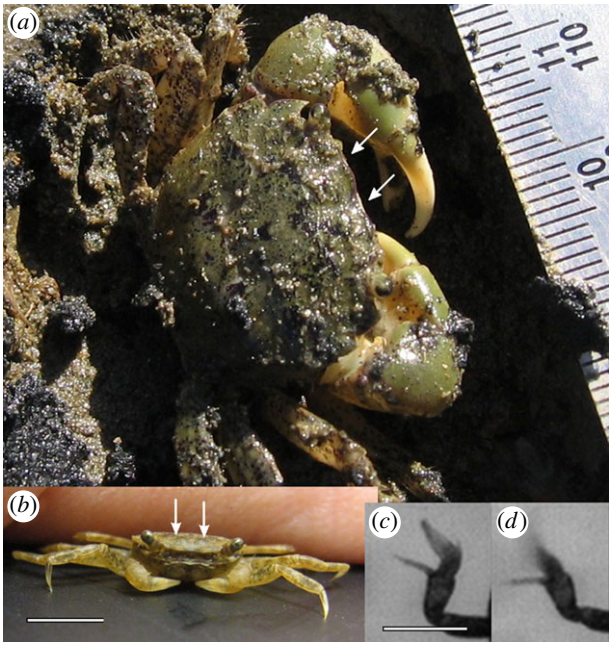

Figure 1. (*a*) Dorsal view of adult (cm ruler) and (*b*) anterior view of juvenile *Hemigrapsus oregonensis*, white arrows indicate locations of first antennae or antennules (scale bar 3 mm). (*c*) Lateral view of antennule during recovery stroke of flicking, showing aesthetascs clumped together; (*d*) lateral view of antennule during downstroke, showing aesthetascs splayed apart (scale bar 1 mm). (Online version in colour.)

1.1. Design of olfactory antennules

In malacostracans, the aesthetascs are arranged in rows on the lateral flagellum of each antennule, with regular spacing between aesthetascs [24–28]. Aesthetascs are hair-like structures innervated by dendrites from chemosensory neurons; the dendrites are surrounded by a thin cuticle, which is permeable to odourants and ions [2,29–35]. The well-studied antennules of lobsters and stomatopods are long with a few stiff aesthetascs in each row [24,25,35].

By contrast, the antennule morphology of brachyuran crabs is considerably different. The flagellum of the antennule is shorter and more compact. Aesthetascs on the antennules of brachyuran crabs are very long compared with other species and flexible. The aesthetascs are arranged in dense toothbrush-like arrays with very little space between neighbouring aesthetascs [15,27,30] (figure 2).

Flicking by crab antennules is divided into two strokes: (i) the rapid downstroke (figure 1*d*) and (ii) the slower return stroke (figure 1*c*) that moves the antennule in the opposite direction [17]. During the flick downstroke of a crab antennule, the aesthetascs are on the upstream side of the antennule and are oriented roughly parallel to the direction of water motion relative to the antennule. During the downstroke, the crab's long, flexible aesthetascs deflect laterally, or 'splay' apart, thereby increasing the widths of the gaps between the aesthetascs. The direction of the slower return stroke is reversed and the aesthetascs, now on the downstream side of the antennule, clump together [17,15,26].

1.2. Fluid dynamics of odour sampling

During flicking, water moves relative to the antennule, while the layer of water in contact with the antennule and aesthetascs does not move relative to their surfaces (the 'no-slip condition') [36]. A velocity gradient (boundary layer) develops between the water moving relative to the aesthetascs and the layer of attached water. The thickness of each boundary layer around an aesthetasc relative to the diameter of the aesthetasc depends on the Reynolds number (*Re*)

$$Re = \frac{Ud\rho}{\mu}, \tag{1.1}$$

where U is the fluid velocity relative to the aesthetasc, d is the aesthetasc diameter, ρ is the fluid density and μ is the dynamic viscosity of the fluid [36]. Higher velocities (and thus higher *Re*'s) during the flick downstroke than during the return stroke lead to thinner boundary layers relative to aesthetasc diameter during the downstroke than the return stroke.

Previous research on fluid dynamics of finite arrays of cylinders describes the relationship between *Re*, the morphology of hair arrays, and the amount of fluid that flows through the gaps between hairs in the array [13,37,38]. The leakiness of an array of cylinders (the volume of fluid that flows through an array of hairs in a unit of time divided by the volume of fluid that would flow through the same area during the same time interval in the absence of hairs) depends on hair *Re*. At $Re \leq 10^{-2}$, leakiness is very low and the spacing between hairs makes little difference, whereas at $Re \approx 0.1$–1, increases in speed or gap width relative to hair diameter can lead to big increases in leakiness [37–39].

The *Re*'s of aesthetascs during antennule flicking by stomatopods [24], spiny lobsters [25] and crabs [17,26], fall within the general range of leakiness sensitivity $0.1 < Re < 1$. For stomatopods [40] and lobsters [41], the aesthetasc arrays are much leakier during the rapid downstroke than during the slow return stroke of flicking antennules. For these antennules, a new sample of water and the odorant molecules it carries should move into the aesthetasc array during the downstroke and then should be trapped between the aesthetascs during the return stroke, giving odourant molecules in the water sample time to diffuse to the surfaces of the aesthetascs [41–43]. Thus, each flick of a lobster or stomatopod antennules is a 'sniff'.

Crab antennules show this asymmetry in stroke speed, but their aesthetascs are much more densely packed than other species. This density is mediated during the downstroke when aesthetascs splay apart, widening the gaps between aesthetascs compared to when they clump together during return strokes [17,26]. Both the asymmetry in speed and changes in gap width suggest that, for adult animals, there should be greater leakiness of crab aesthetasc arrays during the downstroke than during the return stroke [17,26].

1.3. Scaling and the function of antennules

The brachyuran crab, *Hemigrapsus oregonensis* Dana, undergoes a dramatic size change during ontogeny, growing from a juvenile with a carapace width of only 2 mm to an adult with a carapace width of 35 mm (figure 1). There are large differences between the sizes of antennules of juveniles and adults, in addition to the morphological differences observed between crabs and other species, which can affect *Re* if antennules and aesthetascs scale geometrically as the crabs grow. Since the ability of antennules to alter their leakiness, and thus to sniff, depends on operating in the critical *Re* range in which leakiness varies with velocity and gap width, by current models, juvenile crabs may simply be too small to sniff. Therefore, we used *H. oregonensis* to address the question of whether, when, and how the ability to sniff arises during the ontogeny of a crab.

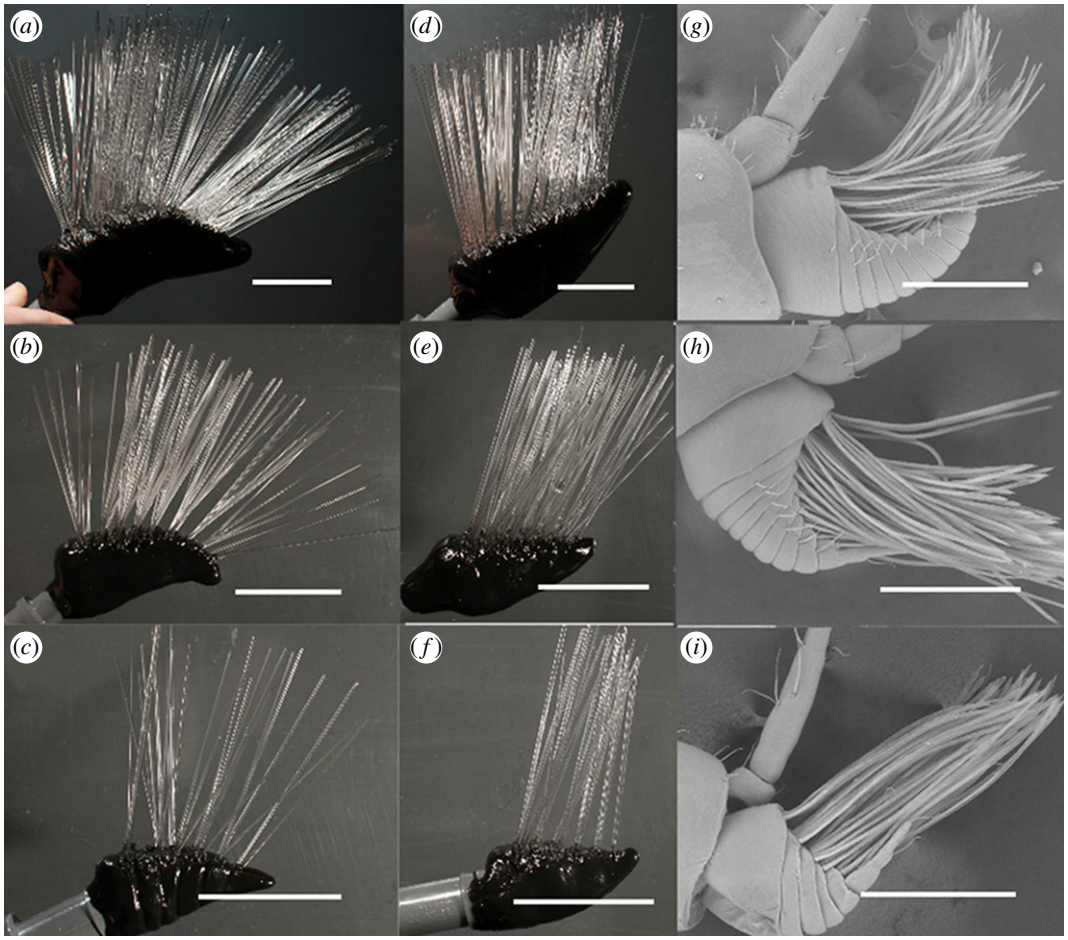

Figure 2. *Hemigrapsus oregonensis* antennules and models. (*a–c*) Dynamically scaled physical models of 'splayed' downstroke. (*d–f*) Dynamically scale physical models of 'clumped' recovery stroke. (*g–i*) Scanning electron micrograph of side view. (*a,d,g*) Adult of 25-mm carapace width, (*b,e,h*) juvenile of 12-mm carapace width and (*c,f,i*) juvenile of 5-mm carapace width. (Online version in colour.)

Antennules and aesthetascs of *H. oregonensis* show allometric scaling as the crabs grow [26]. Aesthetasc diameters are larger relative to carapace width in juveniles than in adults, thus the absolute change in aesthetasc size and *Re* during ontogeny is small. Aesthetasc diameter grows at less than one-third of the rate expected if features remained proportionate through ontogeny.

Changing the gap widths between aesthetascs during growth could also affect fluid flow within a crab's aesthetasc array. The aesthetascs of juvenile *H. oregonensis* are fewer in number and deflect further during the downstroke than the aesthetascs of adults, leading to greater gap widths between aesthetascs for the juveniles than for the adults [26]. These changes in the widths of gaps between aesthetascs during ontogeny can affect the leakiness of the aesthetasc array during antennule flicking.

Although the negative allometry and relatively wider splay ratios are highly suggestive, our previous knowledge of the hydrodynamics of the antennule of a juvenile crustaceans do not allow us to predict how the function of the toothbrush-like antennules of crabs would perform and how performance would vary during ontogeny. Previous studies have investigated sniffing by stomatopods during ontogeny by using only one juvenile model compared to one adult size [24,40]. This approach can account for neither the changing gap width exhibited by crabs during ontogeny nor the potential combined effect of gap width changes and negative allometry in intermediate stages.

1.4. Study objectives

The goal of this study was to quantify the hydrodynamics of flicking by antennules of crabs of different sizes to determine how sniffing performance changes during ontogeny. We used particle image velocimetry (PIV) to measure the fluid flow through aesthetasc arrays of dynamically scaled physical models of antennules of *H. oregonensis* during flick downstrokes and return strokes. The dimensions and *Re*'s of the models, which represented antennules of crabs of six different sizes in an ontogenetic series (carapace widths of 5–25 mm), were based on morphometric and kinematic data from Waldrop [26]. By comparing the volume of fluid entering the aesthetasc arrays during flick downstrokes and return strokes by antennules at different ontogenetic stages, we determined whether they could sniff. The specific questions we addressed were:

(1) At what size are crabs first able to sniff?
(2) How does sniffing performance vary during crab ontogeny?
(3) Do the changes in antennule morphology, flexibility and kinematics that occur during the ontogeny of *H. oregonensis* improve sniffing performance compared with antennules that grow isometrically?

To address this question, we compared our measured flow through aesthetasc arrays for real crabs with calculated estimates of flow through the aesthetascs arrays of antennules

that are geometrically and kinematically similar to the antennules of the largest adults throughout ontogeny, and also for those that maintain the geometry and kinematics of the smallest juveniles as they grow.

2. Material and methods

Water flow through the small, rapidly flicking antennule of a crab is very difficult to quantify directly, so we measured water flow through aesthetasc arrays on larger dynamically scaled physical models of the lateral flagella of antennules of shore crabs, *H. oregonensis*, of different sizes that represent an ontogenetic series from small juveniles to adults.

2.1. Physical models of the antennules

If a model and a real antennule are geometrically similar and operate at the same *Re* (equation (1.1)), they are dynamically similar and the ratios of fluid velocities at comparable positions around the model and the real antennule are the same [36,44,45]. We used the mean values of morphometric and kinematic data reported in [26] to design dynamically scaled physical models of the aesthetasc-bearing lateral filaments of *H. oregonensis* of different sizes (carapace widths of 5, 8, 12, 15, 17 and 25 mm; figure 2*g–i* and table 1). Two models, 'splayed' and 'clumped', of each ontogenetic size were constructed. The splayed configuration of aesthetascs during the downstroke (figure 2*a–c*) was based on the transverse and longitudinal splay ratios (distance spanned by the distal tips of the aesthetascs within the array during the downstroke divided by the width of the aesthetasc array where the aesthetascs insert into the flagellum) measured by Waldrop [26]. The clumped configuration of aesthetascs represented the splay ratio of the aesthetasc arrays during return stroke when the aesthetascs are pushed together (figure 2*d–e*) [26].

The models of antennules of small crabs (carapace widths of 5–12 mm) were scaled up by a factor of 175, and models of larger crabs (carapace widths of 15–25 mm) were scaled up by a factor of 150. The lower scaling factor for larger crabs was used to minimize the possibility of artefacts due to wall effects, as described below (equation (2.1)). Aesthetascs of the appropriate diameter for each model were fabricated out of borosilicate-glass rods (Kugler-Color Clear borosilicate K-100, Friedrich Farbglashütte GmbH, Neugablonz, DE) and inserted into a flagellum made of Sculpey Premo! (Polyform Products Co.) modelling clay. The models were cured at 80°C for 15–30 min, depending on the thickness of the model's flagellum.

2.2. Towing apparatus

We towed our physical models at the *Re*'s of flicking antennules. Models were towed through mineral oil with a density of $\rho = 840\ \mathrm{g\,l^{-1}}$ and a dynamic viscosity of $\mu = 0.049 \pm 0.002$ Pa s ($n = 3$) at 25°C (all experiments were conducted at this temperature). The model was immersed in a 250-l tank (100 cm long, 50 cm wide and 50 cm tall; figure 3*a*). For additional details about the tank and towing set-up, see [41,39]. The model was attached to a towing rig via an arm and towed along rails mounted parallel to the long axis of the tank at *Re*-appropriate speeds by a single-axis microstep-positioning system (MC6023, Daedal Inc., Irwin, PA, USA) controlled by a computer running Matlab. Wall effects can influence the fluid flow around an object at low *Re*, even if the object is relatively far away from the wall [39]. To estimate when wall effects will influence the flow around a body, such as an antennule, a rule of thumb can be used

$$\frac{p}{L} > \frac{20\nu}{LU}, \tag{2.1}$$

where p is the distance between the antennule model and the wall, L is the diameter of antennule model at its widest point, U is the velocity of the body relative to the stationary wall (also the velocity of fluid relative to the aesthetascs) and n is the kinematic viscosity of the fluid, $5.8 \times 10^{-5}\ \mathrm{m^2\,s^{-1}}$ for mineral oil [39]. In our towing experiments, our smallest models had $L = 0.018$ cm and the slowest velocities occurred at $U = 0.0077\ \mathrm{m\,s^{-1}}$, so $y \geq 0.15$ m. For our largest models, $L = 0.034$ m and were towed at a minimum of $U = 0.027\ \mathrm{m\,s^{-1}}$, so $y \geq 0.15$ m or models were positioned at least 0.20 m from each wall at all times, so wall effects were negligible.

2.3. Particle image velocimetry

The mineral oil was seeded with silver-coated glass spheres 11 mm in diameter (Potter Industries, Malvern, PA, USA). Although on average the spheres were neutrally buoyant in mineral oil, some sank or rose through the oil slowly (vertical speed $< 0.2\ \mathrm{mm\,s^{-1}}$), so they travelled less than 0.5 mm during the short duration of each towing experiment. We measured horizontal velocities over a short duration (less than 3 s) so the vertical movements of the particles did not affect our horizontal velocity measurements. The tank was stirred prior to the start of each experiment to ensure the glass spheres were evenly distributed in the mineral oil. We then waited until all motion of the oil in the tank was damped out before beginning each tow.

A laser was used to illuminate a single, horizontal plane that transected each model at its midpoint. The light was produced by a 200-mW laser of wavelength 650 nm (Evolution Series 200, Wicked Lasers, Shanghai, PRC) and fitted with a cylindrical lens that spread the beam into a thin sheet less than 2 mm thick. The laser was mounted to a rigid plate attached to a calibrated microscope stand that could adjust the plate position to the nearest 0.2 mm.

We made video recordings of the motions of the marker particles illuminated by the laser during each tow. The glass aesthetascs had the same refractive index as mineral oil, so we could record the motion of the marker beads within the aesthetasc array without distortion. A high-speed camera (Redlake Inc., Tucson, AZ, USA) was mounted to the towing arm directly above the model and captured the positions of the illuminated glass spheres relative to the model in sequential images (480 × 420 pixels) taken at 60 frames per second. The camera recorded images from the horizontal laser light sheet that captured a cross-sectional view of the model (figure 3*a*).

PIV was used to quantify the fluid flow fields around each dynamically scaled model of an antennule. Sequential pairs of images were processed with MatPIV v. 1.6.2 for Matlab [46] using a method developed by Cowen & Monismith [47]. Each video frame was divided into an array of interrogation windows (8 × 8 pixels), and a cross-correlational analysis technique calculated the most probable displacements of particles. These displacements were used to calculate the local fluid velocity in each sub-window around the model. Images were only selected from the middle third of each towing run.

For each towing run, we analysed 60 image pairs and calculated the mean x and y components of velocity (u and v, respectively) for each sub-window. We replicated each experimental condition three times for each of the 12 models ($n = 3$ replicate runs). The grand mean of u and v in each sub-window was calculated using the mean values for u and v from each run, and the vector sum of each grand mean u and v was used to determine the mean fluid velocity in each sub-window.

Since the areas of the aesthetasc array during the downstroke and return stroke are different, we standardized the velocities within the array (figure 3*b*) to a rectilinear grid (figure 3*c*) so that similar positions within both arrays could be easily compared; S coordinates reflect x-axis positions in the standardized graphs, and T coordinates reflect y-axis positions. Local velocities

Table 1. Summary of morphometrics and kinematics used for each size model based on morphometric analysis in [26]. All antennule and aesthetasc measurements are in metres.

	antennule			aesthetascs			kinematics		
carapace size modelled	length (m)	width (m)	thickness (m)	length (m)	width (m)	total number	*Re* down stroke	*Re* return stroke	Splay ratio side/front
5 mm	1.5×10^{-4}	1.0×10^{-4}	9.7×10^{-5}	3.6×10^{-4}	5.5×10^{-6}	29	0.32	0.13	2.34/4.34
animal	2.6×10^{-2}	1.8×10^{-2}	1.7×10^{-2}	6.2×10^{-2}	9.6×10^{-4}	29	0.32	0.13	
model									
8 mm	1.9×10^{-4}	1.3×10^{-4}	1.3×10^{-4}	4.1×10^{-4}	6.3×10^{-6}	70	0.47	0.20	1.87/3.00
animal	3.3×10^{-2}	2.2×10^{-2}	2.2×10^{-2}	7.2×10^{-2}	1.1×10^{-3}	70	0.47	0.20	
model									
12 mm	2.3×10^{-4}	1.5×10^{-4}	1.6×10^{-4}	4.6×10^{-4}	7.0×10^{-6}	90	0.64	0.30	1.57/2.00
animal	4.1×10^{-2}	2.6×10^{-2}	2.8×10^{-2}	8.1×10^{-2}	1.3×10^{-3}	90	0.64	0.30	
model									
15 mm	2.6×10^{-4}	1.7×10^{-4}	1.9×10^{-4}	5.2×10^{-4}	7.5×10^{-6}	116	0.77	0.38	2.25/2.00
animal	4.9×10^{-2}	2.9×10^{-2}	3.4×10^{-2}	9.0×10^{-2}	1.3×10^{-3}	116	0.77	0.38	
model									
17 mm	2.8×10^{-4}	1.7×10^{-4}	1.9×10^{-4}	5.2×10^{-4}	7.8×10^{-6}	138	0.85	0.42	2.25/2.00
animal	4.9×10^{-2}	2.9×10^{-2}	3.4×10^{-2}	9.0×10^{-2}	1.4×10^{-2}	138	0.85	0.42	
model									
25 mm	3.4×10^{-4}	2.0×10^{-4}	2.4×10^{-4}	5.8×10^{-4}	8.6×10^{-6}	172	1.2	0.62	2.25/2.39
animal	6.0×10^{-2}	3.4×10^{-2}	4.2×10^{-2}	1.0×10^{-1}	1.5×10^{-3}	172	1.2	0.62	
model									

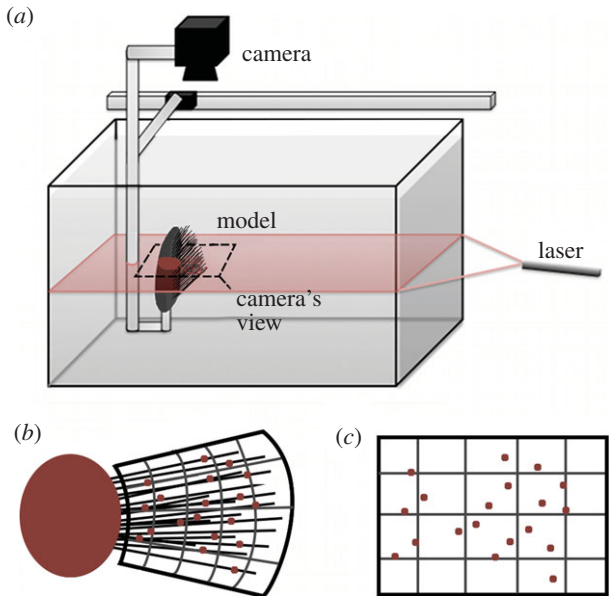

Figure 3. (*a*) Experimental set-up for PIV. The model was mounted to an arm connected to a computer-controlled towing rig that moves the model through a tank containing mineral oil. The long axis of the antennule flagellum was at right angles to the towing direction. Towing velocities produced the *Re*'s of the real antennules during their flick downstroke or return stroke. A camera mounted to the same towing rig travelled with the model, so it recorded fluid motion relative to the model. The glass aesthetascs (black lines) were inserted into the model flagellum at an angle of 35° to the long axis of the flagellum (as shown in figure 2 and diagrammed here). A sheet of laser light (grey) illuminated one plane in the tank, normal to the long axis of the flagellum. The circles (dark grey) on the diagram of the model indicate the sections through the flagellum and the aesthetascs that were in the plane of the light sheet. Because the aesthetascs inserted into the flagellum at an angle of 35°, each aesthetasc crossed into and out of the plane of the laser light at a different point, as indicated by the small circles (dark grey). For simplicity, the diagram shows fewer aesthetascs than are on the real models. (*b*) A cross-section of the model as captured by the camera, which was focused on the plane of the laser sheet. Black lines indicate the aesthetascs, and the dark grey points show where each aesthetasc passed through the laser sheet. (*c*) PIV data within the aesthetasc array after interpolation and transformation (described in the text). Lines of the grid superimposed on the model in (*b*) are now parallel and aesthetasc cross-sections (dark grey) in (*b*) are shown at their transformed positions. (Online version in colour.)

for positions on the standardized grid were interpolated from the PIV velocity vector data using a low-pass interpolation algorithm in Matlab, and the resultant vector for each point was calculated. The colours in figure 4 represented the mean magnitudes of those vectors at each point on the standardized grid ($n = 3$ replicate runs per model).

We used these standardized grids and velocities to calculate the mean water speed in each aesthetasc array. For this calculation, we used the area of the array in which aesthetascs are present. For each run, we used the magnitudes of the velocity vectors at the 6100 grid points within the aesthetasc array to calculate the mean speed of water within the array. PIV data for each carapace width are deposited in Figshare (public data depository): http://dx.doi.org/10.6084/m9.figshare.928567.

2.4. Calculating refreshment of the water sample in an aesthetasc array

Since the aesthetascs of the antennule's array splay apart haphazardly during the downstroke, making a direct calculation of leakiness is impractical. During each downstroke, the aesthetascs have the opportunity to take on a new configuration and therefore change each gap width. For each run, we used the mean, unstandardized velocity vector map to estimate the fraction of the aesthetasc array that was refreshed with a new water sample during a downstroke or a return stroke. A sub-window in the array area was considered refreshed if the parcel of water that was in that sub-window at the beginning of a downstroke or of a return stroke had exited the array by the end of that downstroke or return stroke.

To calculate the fraction of the array that was refreshed, we used a Lagrangian method of tracking fluid parcels with a forward-Euler method of estimating parcel trajectories in Matlab [48]. The code used to run this model can be retrieved from Figshare: http://dx.doi.org/10.6084/m9.figshare.935514. To track fluid parcels, we created an array of evenly spaced points at a constant density (4.5×10^4 points per mm) within the array transformed into real-space coordinates. Assuming the flow was steady and laminar, we divided the duration of the stroke of real animals reported in [26] into time steps of 4.14×10^{-6} s or less in length. Each parcel of water at each time step was advanced a distance determined by multiplying its local velocity by the time step. This process was repeated using the local velocity vector at each new location. At the end of the stroke, the final positions of each parcel of fluid were tested for inclusion within the bounds of the aesthetasc array. Those parcels that moved outside of the array were summed and divided by the total number of parcels that started out in the array to calculate the fraction of the array refreshed. We tested this simulation with a wide variation of time-step lengths and chose the time-step length based on where the simulation converged to a single fraction value.

2.5. Statistical analyses

Two-way analysis of variance (ANOVA) and logit transforms were calculated using the standard statistical package in *R* [49,50]. Significance was determined at the $\alpha = 0.01$ level.

3. Results

3.1. Flow through the aesthetasc array as a function of carapace width

Figure 4 shows examples of maps of velocity vectors that were measured using PIV for three sets of models (figure 2) that represent intermediate growth stages of crabs (juveniles with carapace widths of 5 mm and 12 mm, and an adult with a carapace width of 25 mm). During the downstrokes, all five sets of models we tested experienced high flow velocities within their aesthetasc arrays. By contrast, the return strokes for all models were characterized by very slow velocities within the array, with two exceptions. First, at the very outside edges of the arrays where the tips of the aesthetascs were spread farthest part, fluid velocities were higher than within the rest of the arrays. Second, there was higher variability in the PIV data between replicates for the model of the antennule of the juvenile with a carapace width of 10 mm (figure 5*a*).

Mean water speed within the array is graphed as a function of carapace width in figure 5*a* for downstrokes and return strokes. Mean water speeds within the model array ranged between 0.952 and 3.79 cm s^{-1} for the downstroke condition and 9.86×10^{-3} and 0.352 cm s^{-1} for the return stroke condition. A two-way ANOVA showed that the mean water speed during the downstroke within the aesthetasc array was reliably higher than the recovery stroke ($F_{1,24} = 5337$, $p <$

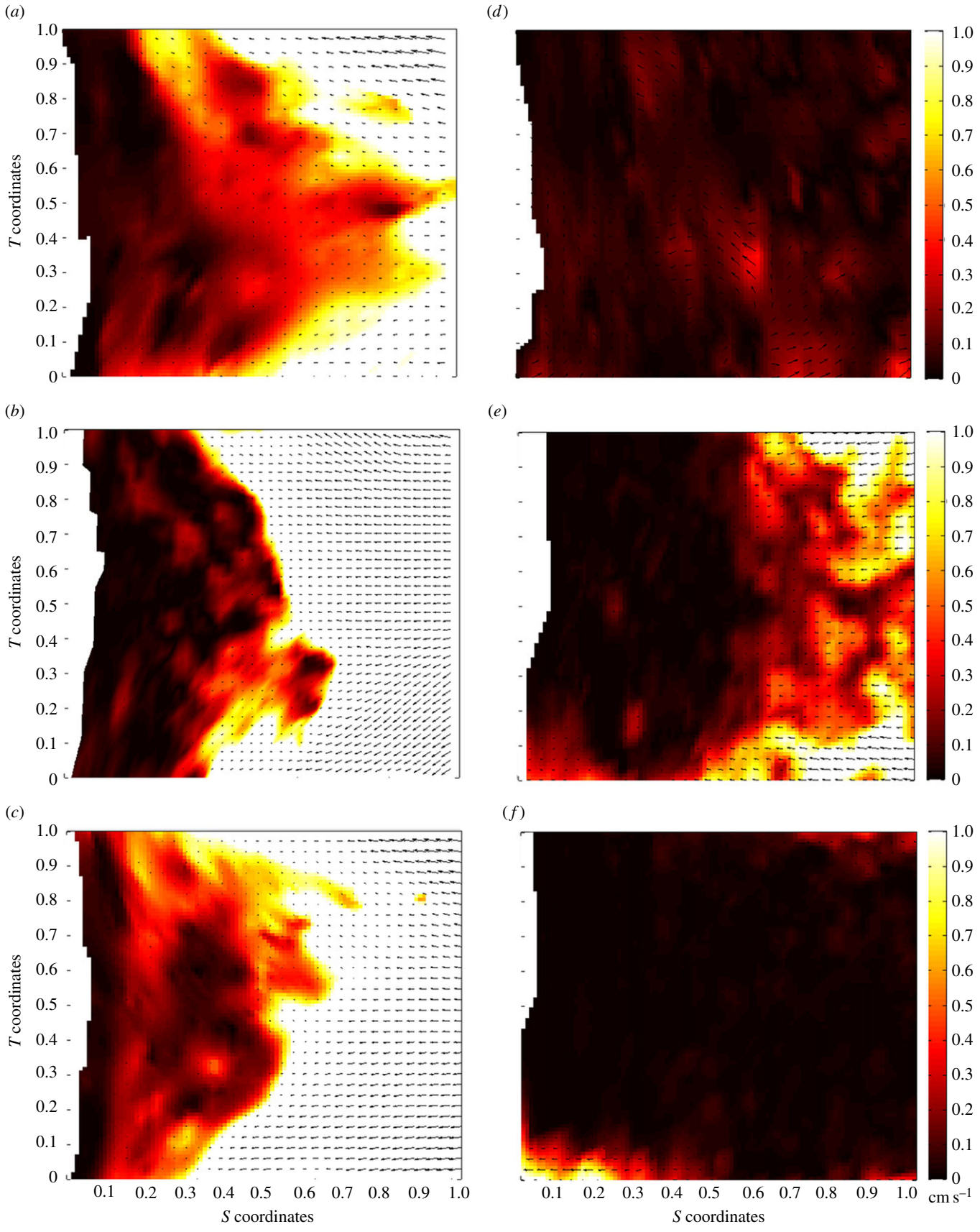

Figure 4. PIV velocity vector maps transformed to the area of the aesthetasc array. (*a–c*) Maps of downstroke conditions and (*d–f*) maps of recovery stroke. (*a,d*) Juvenile of 5-mm carapace width, (*b,e*) large juvenile of 12-mm carapace width, (*c,f*) adult of 25-mm carapace width. All velocity scales are in cm s^{-1}. (Online version in colour.)

2.2×10^{-16}). The downstroke mean water speed also increases significantly with carapace width ($F_{5,24} = 245$, $p < 2.2 \times 10^{-16}$), but the return stroke mean water speed does not ($F_{5,24} = 251$, $p < 2.2 \times 10^{-16}$).

3.2. Fraction of aesthetasc array refreshed during a flick

We calculated the fraction of the model aesthetasc array (figure 4) that was 'refreshed' during a flick downstroke or return stroke (i.e. the area in which water between the aesthetascs was

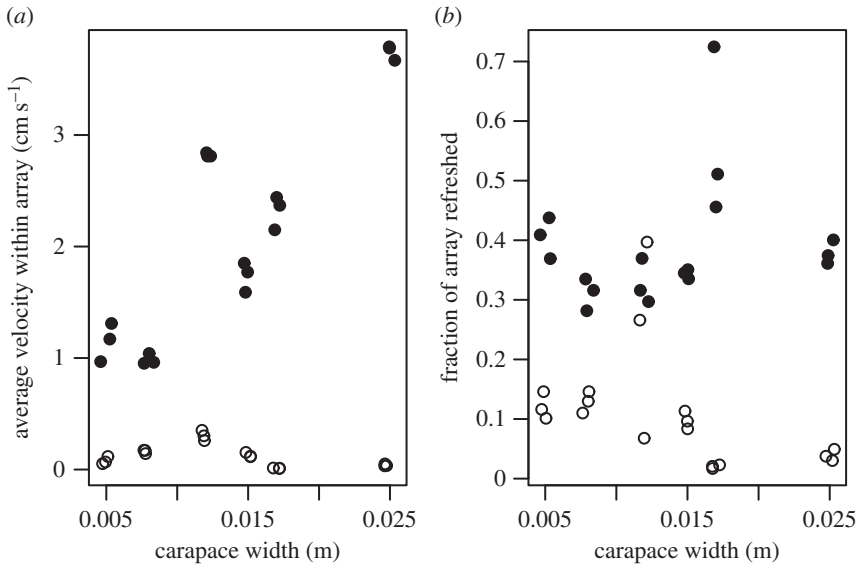

Figure 5. (*a*) Scatter plot of mean water speeds within the aesthetasc array in cm s^{-1} as a function of carapace width. (*b*) Scatter plot of fractions of the aesthetasc array refreshed during the downstroke as a function of carapace width. Filled circles indicate values for the downstroke of the flicking motion; open circles indicate values for the return stroke. All individual replicates are plotted.

washed away and replaced by a new water sample). The fraction of the array refreshed is plotted as a function of crab size (carapace width) in figure 5*b*. Fractions refreshed during the downstrokes ranged from 0.282 to 0.724 and had a mean value of 0.388. By contrast, during the return strokes, all fractions refreshed ranged from 0.017 to 0.397 and had a mean value of 0.108.

Because the dependent variable was a ratio, we used a logit transformation before performing a two-way ANOVA [50]. The ratios were reliably higher for the downstroke than the return stroke ($F_{1,24} = 218$, $p < 1.5 \times 10^{-13}$), but the fraction of the recovery stroke decreased with carapace width ($F_{5,24} = 15.3$, $p = 8.5 \times 10^{-7}$). There was a slight but significant decrease in the ratio with increasing carapace width ($F_{5,24} = 218$, $p = 0.008$).

4. Discussion

4.1. Effects of growth on sniffing performance

Malacostracan crustaceans with long antennules and sparse aesthetasc arrays sniff by flicking their antennules with a rapid downstroke during which water flows into the spaces between the chemosensory aesthetascs on the antennule, and with a slower recovery stroke during which the water sample is trapped within the aesthetasc array (reviewed by Koehl [17]). The ability to change the leakiness of the aesthetasc array to sniff is restricted to a certain range of *Re*'s (equation (1.1)) in which small changes in velocity, aesthetasc diameter or width of the gaps between aesthetascs can cause dramatic alterations in the leakiness of the array [17,37]. In this study, we found that the antennules of crabs with densely packed arrays of aesthetascs also can sniff, and that the aesthetascs of juvenile crabs operate at the very low end of the range of *Re*'s and gap widths in which sniffing by altering array leakiness is effective [27].

Although the model antennules of *H. oregonensis* at all the sizes we studied are able to capture discrete water samples with each flick, our PIV data revealed ontogenetic differences in sniffing performance. For example, compared with the model antennules of smaller crabs, the model antennules of large adult crabs are better at retaining water within the aesthetasc array during flick return strokes. Furthermore, the small size of a juvenile crab's aesthetasc array may lead to more variability between flicks in the amount of fluid exchanged within the aesthetasc array than occurs for large aesthetasc arrays on adult antennules. A likely mechanism for this trend is that small variations in the position of aesthetascs when they splay apart during the downstroke and clump together during the return stroke should have larger effects on fluid exchange in small arrays than in large arrays.

As *H. oregonensis* grows, sniffing performance deteriorates at intermediate size. We found that aesthetasc arrays on the model antennules of crabs with a carapace width of 12 mm experienced lower average velocities during their downstrokes and higher velocities during their return strokes than did arrays on both smaller and larger crabs. The result of these flow patterns is that a greater fraction of the water sample taken during the downstroke is lost during the return stroke for the 12 mm crabs than for smaller or larger crabs (figure 5*b*). This change in sniffing performance could occur as a result of two ontogenetic trends reported by Waldrop [26]. First, splay ratios have a negative relationship with carapace width, so the aesthetascs splay apart more during the downstrokes of small juveniles than of large adults. Second, the average velocities of the downstroke and return stroke have a positive relationships with carapace width, so the antennules of large crabs move more rapidly than those of small crabs. The body size at which the aesthetasc splay ratio becomes adult-like is smaller than the body size at which an antennule acquires the speed and aesthetasc diameter of an adult. Since fluid flow through hair arrays in the *Re* range of crab aesthetascs is extremely sensitive to small changes in inter-hair gap widths and in *Re* (which depends on both hair diameter and speed), it is likely that the different rates at which these features change as crabs grow can cause the observed decline in sniffing performance of mid-sized juvenile crabs.

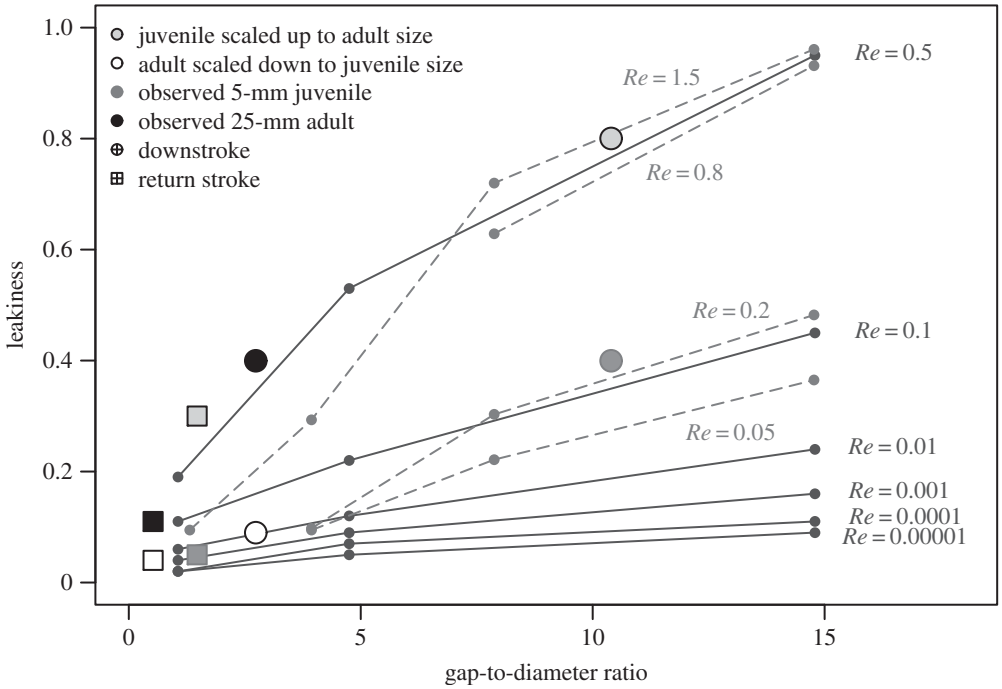

Figure 6. Leakiness (defined in text) of a cylinder array of finite size plotted as a function of the ratio of the width of the gap between adjacent cylinders to the diameter of the cylinders. Each line represents a different *Re*: solid lines based on calculations by Cheer & Koehl [37,38]; dashed lines based on data from Hart [52]. Circles represent flick downstrokes; squares represent return strokes. Leakiness and gap-to-diamater ratio measured for dynamically scaled models of real antennules of adults (25 mm carapace width) are shown by black symbols, and of real juveniles (5 mm carapace width) are shown by dark grey symbols. Isometrically scaled kinematically similar antennules are plotted according to estimates of their *Re* and gap-to-diameter ratio (described in text): light grey symbols represent the antennules of an adult (25 mm carapace width) that is geometrically and kinematically similar to a juvenile (5 mm carapace width). White symbols represent a juvenile (5 mm carapace width) that is geometrically and kinematically similar to an adult (25 mm carapace width).

4.2. Changes in morphology, flexibility and motion during ontogeny

Our data show that the crab *H. oregonensis*, is able to sniff at a wide range of sizes, from tiny juveniles to much larger adults. Waldrop [26] found that the linear dimensions of antennules of *H. oregonensis* increase more slowly than expected relative to increases in carapace width as these crabs grow [26]. Because of this allometric growth, small crabs have larger aesthetascs relative to their body size than do large crabs. Although kinematic data showed that the aesthetascs of juvenile crabs operate at lower *Re*'s than do the aesthetascs of adults, the flexibility of the aesthetascs also changes during ontogeny such that the aesthetascs of small crabs splay apart during the flick downstroke more than do the aesthetascs of large crabs (i.e. the gap widths between aesthetascs is greater for small crabs than for large ones) [26]. This suggests that the net result of juveniles having big aesthetascs relative to body size, and of having large differences between the gap widths during the rapid downstroke and slow recovery stroke of a flick, is that they can sniff.

To ascertain the importance of the changes in morphology, flexibility and flicking kinematics that occur during the ontogeny of the antennules of *H. oregonensis*, we compared our measured leakiness for real antennules with that estimated for antennules that grow isometrically and remain kinematically similar through ontogeny. For isometric growth, antennules at all body sizes must be geometrically similar. Thus, they have the same number and arrangement of aesthetascs at all sizes, and the ratios of linear dimensions of the antennule (e.g. antennule length, aesthetasc diameter) to carapace width is a constant. For flicks to be geometrically similar, then the ratio to carapace width of the distance that the tip of the antennule moves during a flick is constant for all body sizes, and the splay ratio is a constant so that the ratio of gap width to carapace width is the same at all sizes during both the downstroke and the return stroke. If antennules of different sizes are kinematically similar, they must not only have similarity of lengths (geometric similarity), but must also have similarity of corresponding time intervals. Therefore, the ratio of the duration of the flick downstroke to the duration of the return stroke is constant. Since the ratio of carapace width to the distance the aesthetasc-bearing end of the antennule moves is also a constant, the ratio of the downstroke velocity to return stroke velocity is constant for all body sizes.

We considered two cases of isometric growth and kinematically similar flicking: (i) crabs of all sizes have the antennule morphology and kinematics of the largest adult we studied (carapace width of 25 mm) and (ii) crabs of all sizes have the antennule morphology and kinematics of the smallest juvenile we studied (carapace width of 5 mm). Since the duration of the downstroke for real crabs is the same for all body sizes [26], the speeds of the strokes scale linearly with carapace width. We determined the *Re* (equation (1.1)) of each isometric antennule using the calculated aesthetasc diameter for *L* and the calculated velocity for *U*. We then used published values for the leakiness of finite arrays of cylinders with different gap-to-diameter ratios operating at a range of relevant *Re*'s to estimate the leakiness of isometric antennules in each of the cases we considered (figure 6) [37,51]. On a graph of leakiness as a function of gap-to-diameter at various *Re*'s, we have plotted the positions of an 'isometric adult' (25 mm carapace width) that is geometrically and kinematically similar to a very small juvenile (5 mm carapace width). We have also

plotted the measured values of the real adult antennules for comparison. In addition, we have plotted the positions of an 'isometric juvenile' (5 mm carapace width) that is geometrically and kinematically similar to an adult (25 mm carapace width), along with the measured values of the real juvenile antennules for comparison.

Our estimations of the leakiness of isometric antennules indicates that the allometric growth and kinematic changes that occur during the ontogeny of crabs enable them to sniff at all body sizes. If the crabs maintained the adult antennule morphology and motion throughout ontogeny, then small juveniles would not be able to sniff because the leakiness of the aesthetasc array would be too low during the downstroke to permit a new sample of water to be taken between the aesthetascs. If the crabs maintained the juvenile morphology and kinematics throughout ontogeny, then the adult antennule would be very leaky during the return stroke as well as the downstroke. Such an 'isometric adult' could sniff, however, if it paused between flicks so that the water between the aesthetascs at the end of the return stroke could be held long enough for the odorant molecules to diffuse to the aesthetascs.

4.3. Comparison to other crustacean species

Studies of antennule flicking by other malacostracan crustaceans have found that antennules on animals of different sizes can sniff, and that various species maintain the ability to sniff as they grow via different mechanisms. For example, a study of adult lobsters, *Panulirus argus*, showed that they grow allometrically such that lobsters across a range of body sizes have aesthetascs of the same diameter and spacing, and animals of different sizes also flick their antennules at the same speeds [25]. By contrast, a study comparing one juvenile size with one adult size of the stomatopod, *G. mutatus*, showed that adults flick their antennules at higher velocities (which increases leakiness of a hair array), but have more closely spaced aesthetascs (which decreases leakiness) than do smaller juvenile stomatopods, hence the leakiness of both the downstroke and the return stroke of a flick is held constant in spite of a fourfold difference in body size [40]. Unlike lobsters and stomatopods, which have stiff aesthetascs that do not deform during flicking, crabs have flexible aesthetascs that splay apart during the downstroke and clump together during the return stroke [15,17,26]. Like stomatopods, *H. oregonensis* reduce the gap widths between aesthetascs as they grow, but via a different mechanism. The stiffness of the aesthetasc cuticle increases as *H. oregonensis* grows, so the aesthetascs on antennules of larger crabs do not splay apart as much during the flick downstroke as do the more flexible hairs on juvenile antennules [26].

While the earlier studies of size effects on sniffing performance by lobsters and stomatopods did not cover the full range of body sizes, our study of *H. oregonensis* quantified performance at many stages of ontogeny, from newly metamorphosed juveniles to adults. By examining the full range of post-metamorphic growth of these crabs, we found that the *Re*'s of both the downstroke and return stroke of their antennules change by an order of magnitude during ontogeny. However, the *Re*'s at which the crab aesthetascs operate are all within the range of *Re*'s at which leakiness can be altered by small changes in speed, size or hair spacing [37].

4.4. Odour sampling by juveniles of the environment

Since juveniles of *H. oregonensis* co-occur with adults, they share similar predation threats, conspecific interactions and habitat preference as adults [52]. There is evidence that juvenile crabs use chemical cues in order to avoid predation [4] and late-stage larvae use olfaction to detect settlement cues from the environment [53]. Thus, odour capture is an important aspect of crab biology throughout ontogeny. The ontogenetic changes in antennule morphology, flexibility and kinematics probably plays an important role in maintaining the ability of crabs to take discrete samples of their odour environment in space and time.

Acknowledgements. We thank D. Evangelista, S. Khatri and S. Piantadosi for advice on data analysis and statistics; J. Munk for photographs of the physical models and K. Dorgan and E. Robinson for help in the field.

Funding statement. Funds for this study were provided by National Science Foundation grant no. 10S-0842685; James S. McDonnell Foundation grant no. 21002091; the Virginia G. and Robert E. Gill Professorship (to M.A.R.K.); by a National Science Foundation IGERT Traineeship (to L.D.W.); IGERT grant no. DGE-0903711 (to R. Full, M.A.R.K., R. Dudley and R. Fearing); a Sigma-Xi Grant-in-Aid of Research to L.D.W.; by the Undergraduate Research Apprenticeship Program at the University of California, Berkeley and National Science Foundation Research and Training grant no. 5-54990-2311 (to R. McLaughlin, R. Camassa, L. Miller, G. Forest, and P. Mucha).

References

1. Caldwell R. 1979 Cavity occupation and defensive behavior in the stomatopod *Gonodactylus festai*—evidence for chemically mediated individual recognition. *Anim. Behav.* **27**, 194–201. (doi:10.1016/0003-3472(79)90139-8)
2. Gleeson R. 1982 Morphological and behavioral identification of the sensory structures mediating pheromone reception in the blue crab, *Callinectes sapidus*. *Biol. Bull.* **163**, 162–171. (doi:10.2307/1541506)
3. Diaz H, Orihuela B, Forward R, Rittschof D. 1999 Orientation of blue crab, *Callinectes sapidus* (Rathbun), Megalopae: responses to visual and chemical cues. *J. Exp. Mar. Biol. Ecol.* **233**, 25–40. (doi:10.1016/S0022-0981(98)00121-X)
4. Pardieck R, Orth R, Diaz R, Lipcius R. 1999 Ontogenetic changes in habitat use by postlarvae and young juveniles of the blue crab. *Mar. Ecol. Progress Series* **186**, 227–238. (doi:10.3354/meps186227)
5. Zimmer R, Butman C. 2000 Chemical signaling processes in the marine environment. *Biol. Bull.* **198**, 168–187. (doi:10.2307/1542522)
6. Keller T, Powell I, Weissburg M. 2003 Role of olfactory appendages in chemically mediated orientation of blue crabs. *Mar. Ecol. Progress Series* **261**, 217–231. (doi:10.3354/meps261217)
7. Ferner M, Smee D, Chang Y. 2005 Cannibalistic crabs respond to the scent of injured conspecifics: danger or dinner? *Mar. Ecol. Prog. Ser.* **300**, 193–200. (doi:10.3354/meps300193)
8. Shabani S, Kamio M, Derby C. 2009 Spiny lobsters use urine-borne olfactory signaling and physical aggressive behaviors to influence social status of conspecifics. *J. Exp. Biol.* **212**, 2464–2474. (doi:10.1242/jeb.026492)
9. Skog M. 2009 Male but not female olfaction is crucial for intermolt mating in European lobsters (*Homarus gammarus* L.). *Chem. Senses* **34**, 159–169. (doi:10.1093/chemse/bjn073)

10. Lecchini D, Mills S, Brie C, Maurin R, Banaigs B. 2010 Ecological determinants and sensory mechanisms in habitat selection of crustacean postlarvae. *Behav. Ecol.* **21**, 599–607. (doi:10.1093/beheco/arq029)
11. Weissburg M, Zimmer-Faust R. 1994 Odor plumes and how blue crabs use them in finding prey. *J. Exp. Biol.* **197**, 349–375.
12. Moore P, Atema J, Gerhardt G. 1991 Fluid dynamics and microscale chemical movement in the chemosensory appendages of the lobster, *Homarus americanus*. *Chem. Senses* **16**, 663–674. (doi:10.1093/chemse/16.6.663)
13. Koehl M. 2006 The fluid mechanics of arthropod sniffing in turbulent odor plumes. *Chem. Senses* **31**, 93–105. (doi:10.1093/chemse/bjj009)
14. Weissburg M. 2011 Waterborne chemical communication: stimulus dispersal dynamics and orientation strategies in crustaceans. In *Chemical communication in crustaceans* (eds T Breithaupt, M Theil), pp. 63–83. New York, NY: Springer.
15. Snow P. 1973 Antennular activities of hermit crab, *Pagurus alaskensis* (Benedict). *J. Exp. Biol.* **58**, 745–765.
16. Schmitt B, Ache B. 1979 Olfaction: responses of a decapod crustacean are enhanced by flicking. *Science* **205**, 204–206. (doi:10.1126/science.205.4402.204)
17. Koehl M. 2011 Hydrodynamics of sniffing by crustaceans. In *Chemical communication in crustaceans* (eds T Breithaupt, M Theil), pp. 85–102. New York, NY: Springer.
18. Koehl M. 2001 Fluid dynamics of animal appendages that capture molecules: arthropod olfactory antennae. In *Computational modeling in biological fluid dynamics* (eds L Fauci, S Gueron), pp. 97–116. New York, NY: Springer.
19. Mead K, Wiley M, Koehl M, Koseff J. 2003 Fine-scale patterns of odor encounter by the antennules of mantis shrimp tracking turbulent plumes in wave-affected and unidirectional flow. *J. Exp. Biol.* **206**, 181–193. (doi:10.1242/jeb.00063)
20. Keller T, Weissburg M. 2004 Effects of odor flux and pulse rate on chemosensory tracking in turbulent odour plumes by the blue crab, *Callinectes sapidus*. *Biol. Bull.* **207**, 44–55. (doi:10.2307/1543627)
21. Kepecs A, Uchida N, Mainen Z. 2006 The sniff as a unit of olfactory processing. *Chem. Senses* **31**, 167–179. (doi:10.1093/chemse/bjj016)
22. Shoenfeld T. 2006 Special issue: what's in a sniff? the contributions of odorant sampling to olfaction. *Chem. Senses* **31**, 91–92. (doi:10.1093/chemse/bjj014)
23. Reidenbach M, Koehl M. 2011 The spatial and temporal patterns of odors sampled by lobsters and crabs in a turbulent plume. *J. Exp. Biol.* **214**, 3138–3153. (doi:10.1242/jeb.057547)
24. Mead K, Koehl M, O'Donnell M. 1999 Stomatopod sniffing: the scaling of chemosensory sensillae and flicking behavior with body size. *J. Exp. Mar. Biol. Ecol.* **241**, 235–261. (doi:10.1016/S0022-0981(99)00087-8)
25. Goldman J, Koehl M. 2001 Fluid dynamic design of lobster olfactory organs: high speed kinematic analysis of antennule flicking by *Panulirus argus*. *Chem. Senses* **26**, 385–398. (doi:10.1093/chemse/26.4.385)
26. Waldrop L. 2013 Ontogenetic scaling of the olfactory antennae and flicking behavior of the shore crab, *Hemigrapsus oregonensis*. *Chem. Senses* **38**, 541–550. (doi:10.1093/chemse/bjt024)
27. Waldrop L. 2012 *The fluid dynamics of odor capture by crabs*. PhD thesis, University of California, Berkeley, CA, USA.
28. Waldrop L, Bantay R, Nguyen Q. 2014 Scaling of olfactory antennae of the terrestrial hermit crabs *Coenobita rugosus* and *Coenobita perlatus* during ontogeny. *PeerJ* **2**, e535. (doi:10.7717/peerj.535)
29. Gleeson R. 1980 Pheromone communication in the reproductive behavior of the blue crab, *Callinectes sapidus*. *Mar. Behav. Physiol.* **7**, 119–134. (doi:10.1080/10236248009386976)
30. Gleeson R, McDowell L, Aldrich H. 1996 Structure of the aesthetasc (olfactory) sensilla of the blue crab, *Callinectes sapidus*: transformations as a function of salinity. *Cell Tissue Res* **284**, 279–288. (doi:10.1007/s004410050588)
31. Gleeson R, Wheatly M, Reiber C. 1997 Perireceptour mechanisms sustaining olfaction at low salinities: insight from the euryhaline blue crab *Callinectes sapidus*. *J. Exp. Biol.* **200**, 445–456.
32. Hallberg E, Johansson K, Wallen R. 1997 Olfactory sensilla in crustaceans: morphology, sexual dimorphism, and distribution patterns. *int. J. Insect Morphol. Embryol.* **26**, 173–180. (doi:10.1016/S0020-7322(97)00019-6)
33. Gleeson R, Hammar K, Smith P. 2000 Sustaining olfaction at low salinities: mapping ion flux associated with the olfactory sensilla of the blue crab *Callinectes sapidus*. *J. Exp. Biol.* **203**, 3145–3152.
34. Gleeson R, McDowell L, Aldrich H, Hammar K, Smith P. 2000 Sustaining olfaction at low salinities: evidence for a paracellular route of ion movement from the hemolymph to the sensillar lymph in the olfactory sensilla of the blue crab *Callinectes sapidus*. *Cell Tissue Res.* **301**, 423–431. (doi:10.1007/s004410000246)
35. Hallberg E, Skog M. 2011 Chemosensory sensilla in crustaceans. In *Chemical communication in crustaceans* (eds T Breithaupt, M Theil), pp. 103–121. New York, NY: Springer.
36. Vogel S. 1994 *Life in moving fluids: the physical biology of flow*. Princeton, NJ: Princeton University Press.
37. Cheer A, Koehl M. 1987 Paddles and rakes: fluid flow through bristled appendages of small organisms. *J. Theor. Biol.* **129**, 17–39. (doi:10.1016/S0022-5193(87)80201-1)
38. Cheer A, Koehl M. 1987 Fluid flow through filtering appendages of insects. *IMA J. Math. Appl. Med. Biol.* **4**, 185–199. (doi:10.1093/imammb/4.3.185)
39. Loudon C, Best B, Koehl M. 1994 When does motion relative to neighboring surfaces alter the flow-through arrays of hairs. *J. Exp. Biol.* **193**, 233–254.
40. Mead K, Koehl M. 2000 Stomatopod antennule design: the asymmetry, sampling efficiency and ontogeny of olfactory flicking. *J. Exp. Biol.* **203**, 3795–3808.
41. Reidenbach M, George N, Koehl M. 2008 Antennule morphology and flicking kinematics facilitate odour sampling by the spiny lobster, *Panulirus argus*. *J. Exp. Biol.* **211**, 2849–2858. (doi:10.1242/jeb.016394)
42. Stacey M, Mead K, Koehl M. 2002 Molecule capture by olfactory antennules: mantis shrimp. *J. Math. Biol.* **44**, 1–30. (doi:10.1007/s00285050100111)
43. Schuech R, Stacey M, Barad M, Koehl M. 2012 Numerical simulations of odorant detection by biologically inspired sensor arrays. *Bioinspir. Biomim.* **7**, 016001. (doi:10.1088/1748-3182/7/1/016001)
44. Munk J. 2011 *The descent of ant*. PhD thesis, University of California, Berkeley, CA, USA.
45. Evangelista D *et al*. 2014 Aerodynamic characteristics of a feathered dinosaur measured using physical models. Effects of form on static stability and control effectiveness. *PLoS ONE* **9**, e85203. (doi:10.1371/journal.pone.0085203)
46. Sveen J. 2004 *An introduction to MatPIV v. 1.6.1: mechanics and applied mathematics*, 2nd edn. Oslo, Norway: Department of Mathematics, University of Oslo.
47. Cowen E, Monismith S. 1997 A hybrid digital particle tracking velocimetry technique. *Exp. Fluids* **22**, 199–211. (doi:10.1007/s003480050038)
48. Kundu P, Cohen I. 2008 *Fluid mechanics*, 4th edn. Waltham, MA: Academic Press.
49. Team RDC. 2011 *R: a language and environment for statistical computing*. Vienna, Austria: R Foundation for Statistical Computing. (http://www.r-project.org/)
50. Fox J, Weisberg S. 2011 *An R companion to applied regression*, 2nd edn. Thousand Oaks, CA: Sage.
51. Hansen B, Tiselius P. 1992 Flow through the feeding structures of suspension feeding zooplankton: a physical model approach. *J. Plankton Res.* **14**, 821–834. (doi:10.1093/plankt/14.6.821)
52. Hart J. 1935 The larval development of British Columbia brachyura: I. Xanthidae, Pinnotheridae (in part) and Grapsidae. *Can. J. Res.* **12**, 411–432. (doi:10.1139/cjr35-036)
53. Welch J, Rittschof D, Bullock T, Forward R. 1997 Effects of chemical cues on settlement behavior of blue crab *Callinectes sapidus* postlarvae. *Mar. Ecol. Progress Series* **154**, 143–153. (doi:10.3354/meps154143)